



Cite this: *RSC Adv.*, 2023, 13, 23499

# Insight into the effect of fracture surfaces in graphdiyne on the anode performance for lithium ion batteries

Zixuan Zhu \*<sup>a</sup> and Shuke Wang<sup>b</sup>

Two-dimensional (2D) materials are promising anode materials for the next generation of lithium ion batteries. While the Li storage and kinetics at the surface and intercalation sites of 2D materials are widely explored, the effects of the fracture surfaces (FSs) are rarely considered despite the fact that there are numerous FSs in real 2D materials. Herein, we investigate how the FSs in graphdiyne (GDY) affect the anode performance based on first-principles calculations. Results show that both the internal and external FSs have much lower binding energies to Li atoms than perfect GDY, meaning FSs are more active in storing Li atoms. Then, the diffusion barriers of Li atoms on the internal and external FSs are only 0.42 and 0.47 eV, respectively, close to the 0.315 eV of surface sites and lower than the 0.638 eV of intercalation sites, indicating a good kinetics of Li atoms. In addition, due to the new electronic states from the C atoms with dangling bonds, the FSs convert the semiconductor characteristics of perfect GDY to metallic ones, which is helpful to the electronic conductivity. Our work demonstrates that the FSs in 2D materials are beneficial to the anode performance, which may enlighten the design of anode materials.

Received 23rd May 2023  
Accepted 19th June 2023

DOI: 10.1039/d3ra03446a

rsc.li/rsc-advances

## Introduction

The development of the next generation of lithium ion batteries (LIBs) has gained more and more attention with the boom of wireless devices and electric vehicles.<sup>1–3</sup> The flourishing two-dimensional (2D) materials, such as monolayer materials and bulk materials stacked by 2D units, provide additional ideas to upgrade LIBs according to their inherent advantages for ion storage and kinetics. Specifically, 2D materials have natural ion sites and channels at the surface and interlayer<sup>4</sup> unlike alloy anodes<sup>5</sup> where chemical bonds need to be broken when loading and moving the ions, which results in a robust structure during the ion loading/unloading process. In addition, the 2D structures enable their electrochemical properties easily to be turned by doping, and introducing defects and functional groups to adapt to a variety of anode demands.<sup>6,7</sup> Several kinds of 2D materials including graphene and its analogues,<sup>8</sup> carbides and nitrides of transition metals (MXenes),<sup>9</sup> and transition metal dichalcogenides (TMDs)<sup>10</sup> are predicted to be promising anodes for batteries.

Graphdiyne (GDY), a novel 2D material with only carbon, has been widely noted due to the rich chemical structures like benzene rings and acetylenic bonds with sp<sup>2</sup>- and sp-hybridized carbon atoms.<sup>11,12</sup> The electronic states and triangular-like

pores in GDY from the acetylenic linkages can promote ionic storage and migration,<sup>13</sup> which attracts efforts to explore the anode performance of GDY and its derivatives.<sup>14,15</sup> Zhang *et al.*<sup>13</sup> carried out first-principles calculations for the energetics and dynamics of stored Li atoms, and they found the diffusion barrier is only 0.35–0.52 eV and storage capacity as high as that of LiC<sub>3</sub>, which is competitive with a commercial graphite anode. Shang *et al.*<sup>16</sup> prepared ultrathin GDY nanosheets and measured the anode capacity of LIBs, where a ultrahigh capacity of 1388 mA h g<sup>−1</sup> was achieved under a current density of 100 mA g<sup>−1</sup>. Mohajeri *et al.*<sup>15</sup> explored edge-oxidized graphyne and graphdiyne in storing Li atoms with –O, –CO, and –COH as the functional groups. Results showed that functional groups can adjust the band gap from 0.53 to 1.51 eV and significantly affect the anode performances. Mortazavi *et al.*<sup>14</sup> analyzed the stability and anode capacities of N-, P-, As-triphenylene-graphdiyne. These GDY derivatives presented good thermal stability at 2500 K and the capacities can reach 1979 mA h g<sup>−1</sup> and 2664 mA h g<sup>−1</sup> for P- and N-doped structures.

Although there are many theoretical studies of the properties of GDY anodes, a gap between theoretical predictions and experiments is that effects of GDY fracture surfaces (FSs) are rarely considered, which leads to some phenomena in the experiments being difficult to understand. For example, Lu *et al.*<sup>17</sup> showed that a GDY anode keeps a high capacity of 2050 mA h g<sup>−1</sup> after 8000 cycles. However, according to the criterion of the positive open circuit, the first principles calculation predicted that the theoretical capacity of GDY could only

<sup>a</sup>Queen Mary University of London Engineering School, Northwestern Polytechnical University, Xi'an, Shanxi 710072, China. E-mail: zxzhu\_nwpu@126.com

<sup>b</sup>School of Science, China Jiliang University, Hangzhou, Zhejiang 310018, China


reach that of  $\text{LiC}_3$  ( $\sim 744 \text{ mA h g}^{-1}$ ). This may be attributed to the large number of FSs in real materials not being considered in the calculations. Therefore, the present study takes GDY as an example to explore the effect of FSs on the storage and migration of Li atoms. Firstly, the types and structures of FSs are discussed and built. Then, the binding energies to Li, open-circuit voltages and diffusion barriers are obtained. FSs in a GDY anode are found to be beneficial to the capacity and kinetics of Li atoms, and can further improve the anode performance for LIBs.

## Methods

All the properties were calculated by using the density functional theory (DFT) modules implemented in the Vienna *Ab initio* Simulation Package (VASP).<sup>18,19</sup> The generalized gradient approximation (GGA) was employed to evaluate the exchange correlation interactions within the Perdew–Burke–Ernzerhof (PBE) formulation.<sup>20</sup> A kinetic energy cutoff was set to be 520 eV and the *k*-point meshes for the models were automatically generated by vaspkit<sup>21</sup> with a density of 0.03. The DFT-D3 method of Grimme *et al.*<sup>22</sup> including Becke–Johnson damping was used to consider the van der Waals interactions between Li atoms and the GDY FSs. The climbing-image nudged elastic band (CINEB) method<sup>23</sup> in the VASP transition state tools was applied to estimate the diffusion barrier of Li atoms, where 7 images were intercalated into the initial and final positions for the CINEB calculations. A 0.01 eV  $\text{\AA}^{-1}$  threshold was set for the largest force orthogonal to find the lowest diffusion path.

## Results

A real 2D anode material is shown in Fig. 1. As revealed by electron microscopy photos in the literature, 2D electrode materials such as MXenes<sup>24,25</sup> or TMDs<sup>26–28</sup> contain a large number of randomly oriented 2D sheets. The side surfaces of the sheets, which are perpendicular to the 2D layers, are the external FSs. As there are abundant dangling bonds, the storage and transport characteristics for metal ions on the FSs will be different from those of perfect 2D materials. Some 2D sheets include incompletely growing 2D layer, resulting in a smaller size than other layers. Some dangling bonds also exist around

this layer, and the side surfaces of this layer are the internal FSs. The right-hand side of Fig. 1 shows four different positions where ions can be stored in 2D electrode materials, namely intercalation sites, surface sites, internal FS sites, and external FS sites. GDY is taken as an example to explore the effects of the internal and external FSs on the anode performance by comparing with the intercalation and surface sites.

Fig. 2 shows the structures of fractured GDYs with and without Li atoms. When constructing GDY with FSs, a  $2 \times 2$  supercell of GDY with AB stacking mode was firstly constructed. The AB stacking mode is selected because our previous research showed that AB stacking has good structural stability.<sup>29</sup> By removing half of the atoms in a layer of the GDY, the internal FS model can be gained, which is sandwiched between perfect GDY layers. Then, for the external FS, the lattice of the  $2 \times 2$  supercell is added to a 10  $\text{\AA}$  vacuum layer in the in-plane direction instead of deleting any atoms, resulting in the surface adjacent to the vacuum layer becoming the external FS. When conducting structural optimization, the atoms depicted in black circles are fixed during the structural optimization to avoid slippages of the layers. Considering the FS area and the Li atom size, 9 and 18 Li atoms are added in the internal and external FSs, respectively, when calculating the anode properties.

For the internal FS, there was no significant deformation compared to perfect GDY before the adsorption of lithium atoms (Fig. 2a). However, after the adsorption of Li atoms, the FS curls up in the out-of-plane direction (Fig. 2b). For example, two-layer GDY has a distance of 3.375  $\text{\AA}$ , while the curl leads to an interlayer distance of 3.706  $\text{\AA}$  at the FS. The charge transfer between Li and C atoms around the FS can break the original electron cloud and enable the deflection of the covalent bonds. As a contrast, the perfect layer of GDY keeps in a plane, meaning a higher stability and weaker interaction with Li atoms. As to the external FS, the triangular-like pore adjacent to FS becomes oval (Fig. 2c), meaning a change of the bond types. Specifically, the two C atoms at the triangle vertex originally belong to a hexatomic ring with partial double bond. Whereas, in the FS the bonds related to the two C atoms will become alternate single bond and triple bond like an alkyne, which makes the variant of a triangular-like pore. Then, the adsorption of Li atoms can also result in the warping of the external FS. Importantly, although

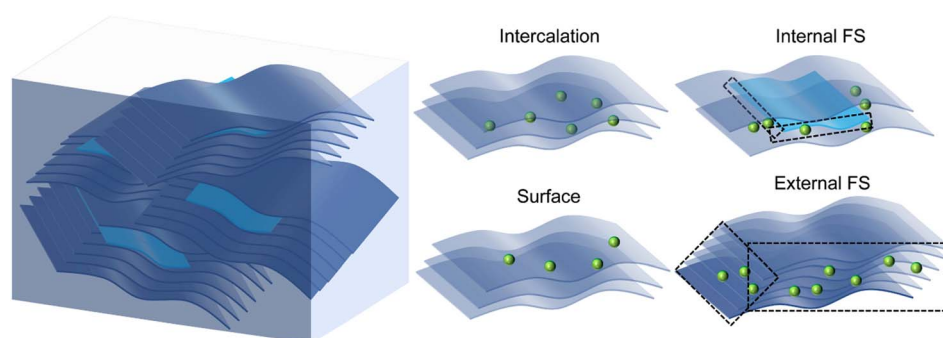


Fig. 1 Typical fracture surfaces (FS) in a real 2D anode material and possible Li atom positions, where the FSs are marked by the black dashed boxes.



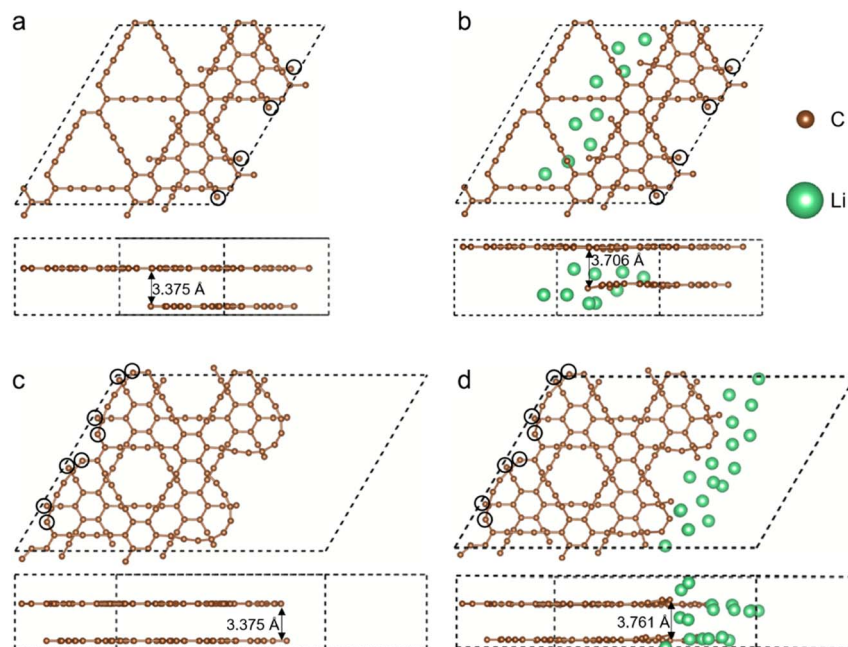


Fig. 2 Geometry optimization of FSs in GDYs with and without Li atoms: (a) internal FS without Li atoms, (b) internal FS with Li atoms, (c) external FS without Li atoms, and (d) external FS with Li atoms. The fixed atoms during the optimization are marked by black circles, and arrows indicating distances are used to show the curls of FSs.

the FSs are slightly deformed because of Li adsorption, the boundary atoms do not break away from the GDY, meaning the FS can stably store Li atoms.

To analyze the effects of FSs on the anode performance, the binding energy,  $E_b$ , to Li atoms and the open-circuit voltage,  $V$ , are defined as follows:

$$E_b = \frac{E(\text{FS} + n\text{Li}) - E(\text{FS}) - nE(\text{Li})}{n}, \quad (1)$$

$$V(n) = \frac{-E(\text{FS} + n\text{Li}) + E[\text{FS} + (n-1)\text{Li}] + E(\text{Li})}{e}, \quad (2)$$

where  $E(\text{FS} + n\text{Li})$ ,  $E(\text{FS})$  and  $E(\text{Li})$  are the total energies of FS with  $n$  adsorbed Li, only FS, and only a Li atom in the most stable crystal, respectively,  $n$  is the number of adsorbed Li atoms, and  $e$  is the charge quantity of an electron. As shown in Fig. 3a and b, the charge density isosurfaces indicate that Li and C atoms have clear charge exchange. For example, the blue isosurfaces of the adjacent Li and C atoms are generally shared. The Li atoms far away from the FS usually have isolated charge density isosurfaces, meaning weaker adsorptions than those closer to the FS. In addition, although Li atoms on the internal FS can be near to the C atoms both in the FS and in the perfect GDY, the shared isosurfaces are more common for the Li atoms and C atoms in the FS. Therefore, the FS might be more active in storing Li atoms.

The quantitative evaluations of the anode performance of FSs are shown in Fig. 3c and d. The binding energy of Li and average voltage for perfect AB stacked GDY with  $\text{LiC}_6$  configuration are also shown for comparison. With the increase of Li number, the binding energy of Li atoms almost linearly

increases from  $-2.6$  eV to  $-1.95$  eV for the internal FS (Fig. 3c). As lower  $E_b$  means stronger adsorption, the increase of  $E_b$  could be owing to the Coulomb repulsion between the Li atoms weakening the adsorption to the newly added Li atom. Compared to the binding energy of  $-1.12$  eV of Li atoms on perfect GDY, the much lower  $E_b$  of FS means the C atoms with dangling bonds can more closely bond with Li atoms than those in perfect GDY. Therefore, although the open-circuit voltage of the internal FS decreases from 2.6 to 1.31 V, it is always higher than the average voltage of perfect GDY (0.74 V). As to the external FS, the binding energy of Li atoms and open-circuit voltage are similar to those of the internal FS, while the binding energy becomes higher, indicating a slightly weaker adsorption (Fig. 3d). That may be because the Li atom on the internal FS can feel the attractions from both the FS and the perfect GDY layer, but that on the external FS can only be attracted by the FS. In general, both the FSs can store Li atoms and the bonds to Li atoms are stronger than for perfect GDY, which may explain the much higher capacity of the real GDY anode<sup>30,31</sup> than the theoretical prediction with the abundant FSs in a real GDY anode providing additional sites for Li storage.

In addition to the storage of Li atoms, the kinetics of Li atoms on the FSs is also discussed by using CINEB calculations as shown in Fig. 4. The initial and final positions of each Li atom are obtained from the geometry optimization, and seven images are intercalated into the path. The lowest energy paths for Li diffusion are displayed in Fig. 4a for internal FS and Fig. 4b for external FS. During the migration, the energy of the Li atom has a peak of 0.42 eV on the internal FS, meaning that diffusion can be achieved only when overcoming a barrier of 0.42 eV. While for the external FS, the energy barrier increases to



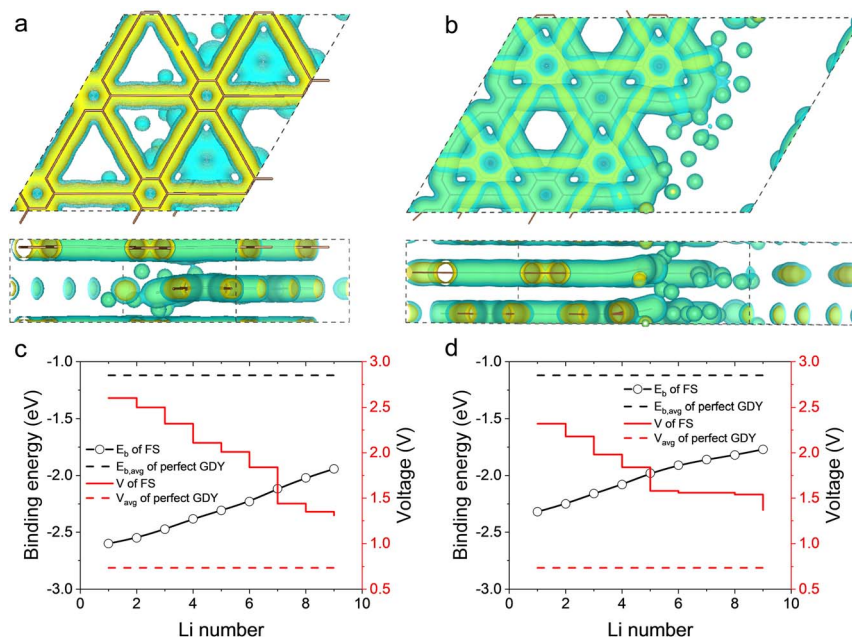


Fig. 3 Binding energy of Li atoms on the FSs in GDYs, where (a) and (b) are charge densities of internal FS with Li atoms and external FS with Li atoms, and (c) and (d) are the binding energies and open-circuit voltages of internal and external FSs when storing Li atoms. Yellow and blue in (a) and (b) indicate the isosurfaces with higher and lower density values.

about 0.47 eV. The lower barrier of the internal FS might result from the adjacent perfect GDY layer, which offers a relatively flat path for Li atom diffusion. Comparing to the intercalation and surface sites, where the energy barriers are 0.638 and 0.315 eV,<sup>29</sup> the FS sites have moderate resistance for the migration of Li atoms. We summarize the anode performances of internal and external FSs and compare them to that of perfect GDYs in Table

1. As the FSs provide additional Li sites, which have greater attraction to Li, the FSs are expected to enhance the capacity.

The electronic conductivity of an anode is also important to LIB performance.<sup>32</sup> Therefore, the density of states (DOSs) of internal and external FSs before and after Li adsorptions are obtained to evaluate the electronic conductivities. Previous DFT calculations<sup>33,34</sup> showed perfect GDY has a band gap of 0.46–

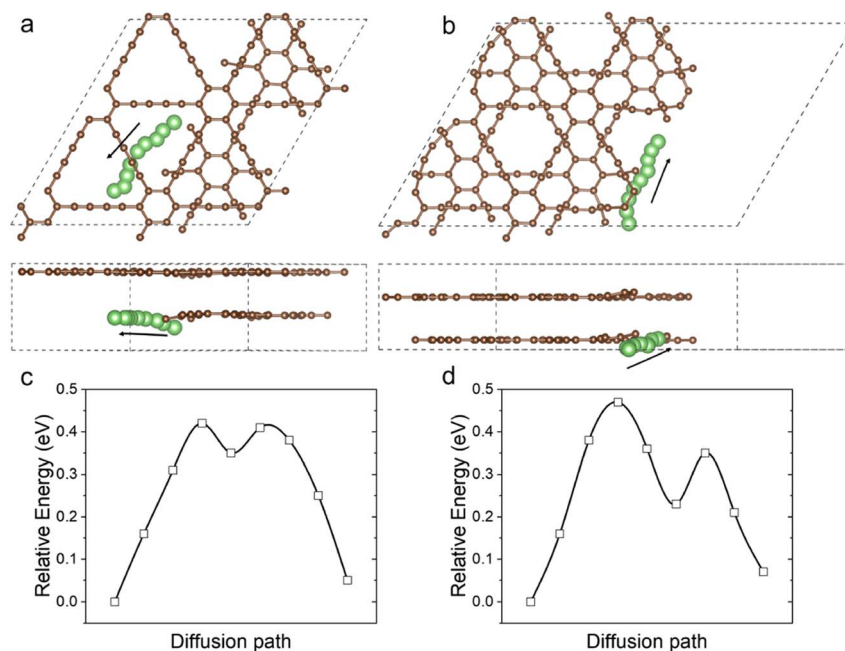


Fig. 4 Diffusion barriers of Li atoms on the FSs in GDYs, where (a) and (b) are the diffusion paths of Li atoms on internal and external FSs, respectively, and (c) and (d) are the corresponding energy profiles. The arrows show the directions of Li migration.





Table 1 Comparison between the anode performances of FSs and perfect GDYs

Structure	Average binding energy (eV)	Highest voltage (V)	Average voltage (V)	Diffusion barrier (eV)
Internal FS	−2.29	2.60	1.94	0.42
External FS	−2.02	2.32	1.77	0.47
Monolayer GDY <sup>29</sup>	−1.12	1.80	0.736	0.315
Stacking GDY <sup>29</sup>	Not reported	Not reported	Not reported	0.638

1 eV, meaning a semiconductor characteristic. However, both the GDY FSs (Fig. 5a and c) present nonzero DOSs at the Fermi level, presenting a metallic characteristic. The nonzero DOSs might be because some new states are introduced into the band gap by the C atoms with dangling bonds. Actually, like graphene ribbons that have different electronic band structures from that of perfect graphene,<sup>35,36</sup> the defects due to vacancies can induce metallization and even magnetization in nonmagnetic semiconducting nanoribbons due to the spin polarization of local defect states. In addition, after adsorbing Li atoms, the DOSs at the Fermi level are increased compared to pristine FSs due to the charge transfer from Li to C atoms, meaning a better electronic conductivity. Therefore, the DOSs at the FSs indicate that the existence of FSs in the GDY anode is beneficial to the electronic conductivity.

As the above results confirmed the FSs have a significant effect on the anode capacity, two questions may appear as to how to experimentally quantify and control the FSs in 2D anode materials and whether the FS results in more irreversible

capacity. For the first question, imaging with a scanning electron microscope (SEM) can intuitively present the FSs. Analyzing enough SEM images, the density of FSs may be obtained. In addition, Raman spectra can reflect the lattice vibration of a specific frequency. If there are some typical functional groups around the FSs, using the peak intensity, corresponding peak positions may be used to derive the density of FSs. In addition, treatments in extreme conditions,<sup>28</sup> including acid and base corrosion or high-temperature sintering, could introduce FSs in 2D materials. For the second question, we think the FSs will not create more irreversible capacity. On the one hand, the highest voltage of FS reaches  $\sim 2.6$  V, which is not higher than that of generally used anode materials like  $V_2CO_2$  (3.0 V).<sup>37</sup> On the other hand, the diffusion barrier of Li on the FS is close to the barriers in intercalation and surface sites. Therefore, during the discharge of the anode, the stored Li on the FS can be easily released and thus lead to working in cycles.

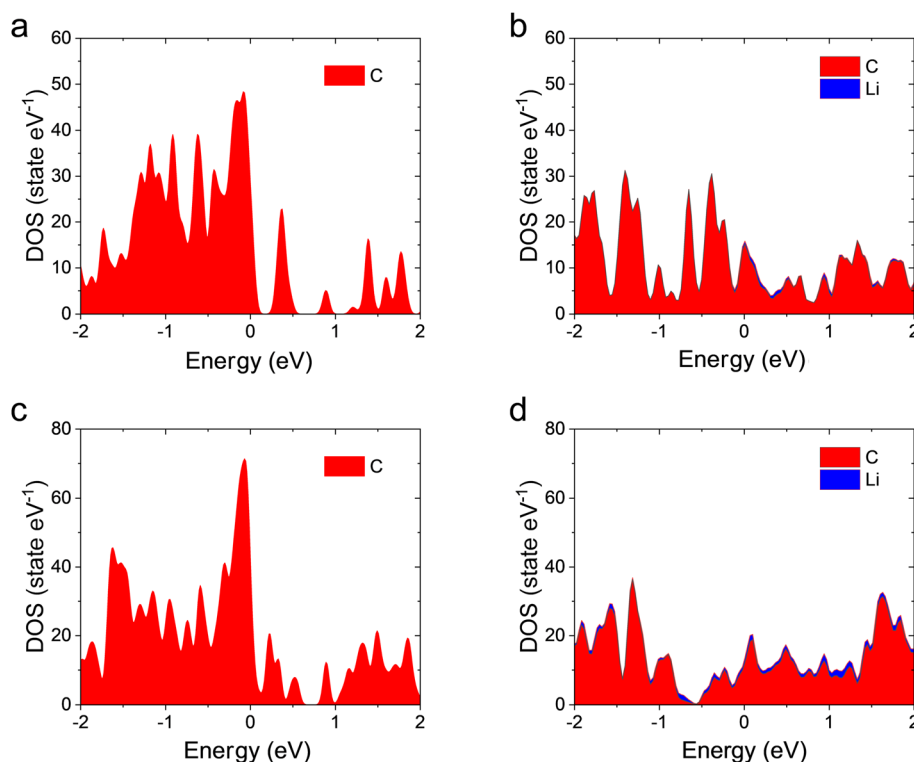


Fig. 5 Density of states (DOSs) of FSs in GDYs with and without Li atoms: (a) internal FS without Li atoms, (b) internal FS with Li atoms, (c) external FS without Li atoms, and (d) external FS with Li atoms. The red and blue indicate the contributions of C and Li atoms to the DOSs.

## Conclusions

In this study, the effects of FSs on the anode performance of GDY for LIBs are investigated by using first-principles calculations. Internal and external FSs were constructed based on a  $2 \times 2$  supercell of GDY with AB stacking mode. The geometry optimizations indicate that although the GDY FSs can be slightly deformed due to Li adsorption, they can stably store Li atoms without destruction. The FSs have stronger attractions to Li atoms than perfect GDY, with the Li atom binding energy of internal FS being from  $-2.6$  to  $-1.95$  eV with increasing Li number, much lower than the  $-1.12$  eV of perfect GDY. The lower binding energy also results in a higher open-circuit voltage (from 2.6 to 1.31 V) than the average voltage of perfect GDY (0.74 V). Therefore, the FSs are more active in storing Li atoms and also beneficial for the capacity improvement of the GDY anode. Then, the diffusion barriers of Li atoms on the internal and external FSs were calculated based on the CINEB method. Results show the barriers on the internal and external FSs are only 0.42 and 0.47 eV, respectively, close to the 0.315 eV of surface sites and lower than the 0.638 eV of intercalation sites. Although perfect GDY is a semiconductor, the DOSs of the FSs have nonzero values at the Fermi level due to the new states introduced into the band gap by the C atoms with dangling bonds, which can facilitate electronic transport. Therefore, this work manifests that the FSs in a GDY anode increase the capacity and kinetics of Li atoms and enhance the electronic conductivity, which can further improve the anode performance for LIBs.

## Conflicts of interest

There are no conflicts to declare.

## References

- M. Li, J. Lu, Z. Chen and K. Amine, *Adv. Mater.*, 2018, **30**, 1800561.
- J. B. Goodenough, *Energy Storage Mater.*, 2015, **1**, 158–161.
- D. Song, X. Chen, Z. Lin, Z. Tang, W. Ma, Q. Zhang, Y. Li and X. Zhang, *ACS Nano*, 2021, **15**, 16469–16477.
- Y. Wu and Y. Yu, *Energy Storage Mater.*, 2019, **16**, 323–343.
- J. Liu, P. Kopold, P. A. van Aken, J. Maier and Y. Yu, *Angew. Chem., Int. Ed.*, 2015, **54**, 9632–9636.
- R. Rojaee and R. Shahbazian-Yassar, *ACS Nano*, 2020, **14**, 2628–2658.
- P. Luo, F. Zhuge, Q. Zhang, Y. Chen, L. Lv, Y. Huang, H. Li and T. Zhai, *Nanoscale Horiz.*, 2019, **4**, 26–51.
- R. Mukherjee, A. V. Thomas, D. Datta, E. Singh, J. Li, O. Eksik, V. B. Shenoy and N. Koratkar, *Nat. Commun.*, 2014, **5**, 3710.
- C. J. Zhang, S. Park, A. Seral-Ascaso, S. Barwich, N. McEoy, C. S. Boland, J. N. Coleman, Y. Gogotsi and V. Nicolosi, *Nat. Commun.*, 2019, **10**, 849.
- S. Li, H. Tang, P. Ge, F. Jiang, J. Zhou, C. Zhang, H. Hou, W. Sun and X. Ji, *ACS Appl. Mater. Interfaces*, 2018, **10**, 6378–6389.
- G. Li, Y. Li, H. Liu, Y. Guo, Y. Li and D. Zhu, *Chem. Commun.*, 2010, **46**, 3256.
- L. Sun, P. H. Jiang, H. J. Liu, D. D. Fan, J. H. Liang, J. Wei, L. Cheng, J. Zhang and J. Shi, *Carbon*, 2015, **90**, 255–259.
- H. Zhang, Y. Xia, H. Bu, X. Wang, M. Zhang, Y. Luo and M. Zhao, *J. Appl. Phys.*, 2013, **113**, 44309.
- B. Mortazavi, M. Shahrokhi, M. E. Madjet, M. Makaremi, S. Ahzi and T. Rabczuk, *Carbon*, 2019, **141**, 291–303.
- A. Mohajeri and A. Shahsavari, *Comput. Mater. Sci.*, 2016, **115**, 51–59.
- H. Shang, Z. Zuo, L. Li, F. Wang, H. Liu, Y. Li and Y. Li, *Angew. Chem., Int. Ed.*, 2018, **57**, 774–778.
- T. Lu, J. He, R. Li, K. Wang, Z. Yang, X. Shen, Y. Li, J. Xiao and C. Huang, *Energy Storage Mater.*, 2020, **29**, 131–139.
- G. Kresse, *J. Non-Cryst. Solids*, 1995, **193**, 8.
- G. Kresse and J. Furthmüller, *Comput. Mater. Sci.*, 1996, **6**, 15–50.
- J. P. Perdew, K. Burke and M. Ernzerhof, *Phys. Rev. Lett.*, 1996, **77**, 3865–3868.
- V. Wang, N. Xu, J. Liu, G. Tang and W. Geng, *Comput. Phys. Commun.*, 2021, **267**, 108033.
- S. Grimme, J. Antony, S. Ehrlich and H. Krieg, *J. Chem. Phys.*, 2010, **132**, 154104.
- G. Henkelman, B. P. Uberuaga and H. Jónsson, *J. Chem. Phys.*, 2000, **113**, 9901–9904.
- Y. Sun, D. Chen and Z. Liang, *Mater. Today Energy*, 2017, **5**, 22–36.
- B. Anasori, M. R. Lukatskaya and Y. Gogotsi, *Nat. Rev. Mater.*, 2017, **2**, 16098.
- M. Ma, S. Zhang, Y. Yao, H. Wang, H. Huang, R. Xu, J. Wang, X. Zhou, W. Yang, Z. Peng, X. Wu, Y. Hou and Y. Yu, *Adv. Mater.*, 2020, 2000958.
- C. Chen, X. Xie, B. Anasori, A. Sarycheva, T. Makaryan, M. Zhao, P. Urbankowski, L. Miao, J. Jiang and Y. Gogotsi, *Angew. Chem., Int. Ed.*, 2018, **130**, 1864–1868.
- J. Zhou, L. Wang, M. Yang, J. Wu, F. Chen, W. Huang, N. Han, H. Ye, F. Zhao, Y. Li and Y. Li, *Adv. Mater.*, 2017, **29**, 1702061.
- Z. Zhu and D. Song, *ACS Omega*, 2023, **8**, 8441–8447.
- X. Ren, X. Li, Z. Yang, X. Wang, J. He, K. Wang, J. Yin, J. Li and C. Huang, *ACS Sustainable Chem. Eng.*, 2020, **8**, 2614–2621.
- Y. Liu, Y. Qing, B. Zhou, L. Wang, B. Pu, X. Zhou, Y. Wang, M. Zhang, J. Bai, Q. Tang and W. Yang, *ACS Nano*, 2023, **17**, 2431–2439.
- C. Sevik and D. Çakır, *Phys. Rev. Appl.*, 2019, **12**, 014001.
- M. Long, L. Tang, D. Wang, Y. Li and Z. Shuai, *ACS Nano*, 2011, **5**, 2593–2600.
- H. Bu, M. Zhao, H. Zhang, X. Wang, Y. Xi and Z. Wang, *J. Phys. Chem. A*, 2012, **116**, 3934–3939.
- M. Topsakal, E. Aktürk, H. Sevinçli and S. Ciraci, *Phys. Rev. B: Condens. Matter Mater. Phys.*, 2008, **78**, 235435.
- S. S. Chauhan, P. Srivastava and A. K. Shrivastava, *Solid State Commun.*, 2013, **154**, 69–71.
- M. Naguib, J. Halim, J. Lu, K. M. Cook, L. Hultman, Y. Gogotsi and M. W. Barsoum, *J. Am. Chem. Soc.*, 2013, **135**, 15966–15969.

